

# STRUCTURAL AND UPCONVERSION PROPERTIES OF $\text{Er}^{3+}$ AND $\text{Yb}^{3+}$ CO-DOPED $\text{Y}_2\text{Ti}_2\text{O}_7$ PHOSPHORS

---

## 3.1 Introduction

In recent years, efforts are being concentrated on the  $\text{Er}^{3+}$  doped glasses/crystals as UC lasers and powder phosphors as random lasers that could emit light in the green, blue and UV regions of the optical spectrum.  $\text{Er}^{3+}$  is a suitable ion for the UC process because of its favourable energy level structure. However, the high phonon energy corresponding to the stretching vibrations of the oxide bond generally acts as a constraint in obtaining efficient UC. Hosts with low phonon energy can reduce the non-radiative losses due to lower multi-phonon relaxation (MPR) rates and thus could enhance the UC signal [Auzel (2004)] Rare earth doped  $\text{Y}_2\text{Ti}_2\text{O}_7$  belonging to pyrochlore family attracted a great deal of attention due to its intriguing optical properties such as laser material, temperature sensor, photo catalytic properties as energy storage, electrolyte material in solid oxide fuel cells (SOFC). [Singh, et al. (2013), Gill, et al. (2012)]. UC efficiency is greatly enhanced in the presence of  $\text{Yb}^{3+}$  ion because of its higher absorption cross section to  $\text{Er}^{3+}$  ion. Main mechanisms which influence the fluorescent centers in any material are:

1. Interaction of ligand crystal field, its intensity related to the electrostatic field strength;  $Ze/r^2$ .
2. Interaction of the phonon field of the matrix, determining the Transition probabilities, line widths and quantum efficiency of fluorescent centers.
3. Interaction with other impurity centers capable of energy transfer to or from the fluorescent center. [Bhargava, et al. (1997)].

There is growing interest in the development of new full color emitting phosphor materials that combine thermal and chemical stability in air with high emission quantum yield at room-temperature. In order to fulfill the corresponding requirements in various application fields, many research papers on developing new up-conversion materials systems have been reported. Recently, the researches on rare earth ions doped up-conversion luminescence materials have received a considerable attention because of their peculiar optical properties arising from the intra 4f transitions. These luminescent properties of lanthanides make them useful for applications in flat-panel display, solid-state

laser, optics, optical telecommunication, temperature sensor, as light emitting diodes and *in vitro* and *in vivo* applications [Zheng, et al. (2010), Parchur, et al. (2012a), Parchur, et al. (2011a), Raju, et al. (2012), Auzel (2004), Wang, et al. (2009), Hoppe (2009), Chen, et al. (2009), Wang, et al. (2005)]. Among others, special attention has been given to rare-earth doped hosts emitting in the visible range upon infrared excitation up-conversion process [Patra, et al. (2002), Yi and Chow (2005), Chen, et al. (2008), Yang, et al. (2010), Liu, et al. (2001), Chen, et al. (2012)]. Co-doping with  $\text{Yb}^{3+}$  as sensitizer further increases the efficiency of the up-conversion process through donor–acceptor processes in rare earths like  $\text{Tm}^{3+}$ ,  $\text{Ho}^{3+}$ ,  $\text{Er}^{3+}$  ions [Chung, et al. (2012), Li, et al. (2011), Quin, et al. (2007), Yan, et al. (2012)]. The combined  $\text{Er}^{3+}/\text{Yb}^{3+}$  doped low phonon energy host matrices are of special interest, wherein the up-conversion process results into efficient blue, green, and red emissions. The large spectral overlap between  $\text{Yb}^{3+}$  emission ( ${}^2\text{F}_{5/2} \rightarrow {}^2\text{F}_{7/2}$ ) and  $\text{Er}^{3+}$  absorption ( ${}^4\text{I}_{15/2} \rightarrow {}^4\text{I}_{11/2}$ ) is responsible for such efficient resonant energy transfer (ET) from  $\text{Yb}^{3+}$  to  $\text{Er}^{3+}$  [Patra, et al. (2003), Matsuuara (2002), Kink, et al. (1999)]

Among the up-conversion phosphor materials, pyrochlore titanates  $\text{Y}_2\text{Ti}_2\text{O}_7$  (YTO) has attracted attention due to its thermal stability, low phonon energy ( $\sim 712 \text{ cm}^{-1}$ ), photocatalytic behaviour and high refractive index value ( $\sim 2.34$ ) [Dai, et al. (2012), Fuentes, et al. (2005), Abe, et al. (2006), Ting, et al. (2011)]. The optical band gap of host material  $\text{Y}_2\text{Ti}_2\text{O}_7$  is  $\sim 3.7 \text{ eV}$ . This wide band gap of the host reduces a quenching effect on the emission of  $\text{Ln}^{3+}$  ion. The  $\text{Ln}^{3+}$  ion doped phosphor gives colours in blue, green and red regions. In particular co-doping effects on  $\text{Ln}^{3+}$  emission is critically dependent on structure of host matrix, excited state absorption (ESA) and energy transfer (ET) between the f–f transitions of  $\text{Er}^{3+}$  and/or  $\text{Er}^{3+}/\text{Yb}^{3+}$  combined system. Particularly owing to advances in IR sources, up-conversion process green/red phosphors are of special subject of interest. Therefore, systematic research on synthesis mechanism, structure and resultant effects on phosphor characteristics is necessary and worthy of pursuit. Among the solution based synthesis methods the conventional solid-state reaction method is one of the versatile and low cost techniques to prepare the up-conversion phosphor materials. The major drawback in this method is that it is not easy to control the particle size and morphology at higher sintering temperatures [Pan, et al. (2012)]. However, the sample prepared at higher temperature ( $\sim 1200 \text{ }^\circ\text{C}$ ) for long duration ( $\sim 12 \text{ h}$ ) shows strong photoluminescence because of less number of quencher on the surface of the particles, which is due to the possibility of reduced dangling bonds on the particle surface. Recently, this problem in nanomaterials is

reduced by annealing the as prepared sample at higher temperature [Parchur, et al. (2012b)]. Recently, Cheetham, et al.(2011) prepared  $Yb^{3+}$ ,  $Er^{3+}$  and  $Tm^{3+}$  co-doped  $Y_2BaZnO_5$  phosphors at  $\sim 1200$  °C and sintered for several days. Samples show strong green, red, blue and white emission depending on proportion of the rare earth ions.

It is interesting to see that these samples are excited at very low power ( $\sim 25-90$  mW/mm<sup>2</sup>) [Etchart, et al. (2011), Etchart, et al. (2010)]. Moreover, preparation method of colloidal/hybrid nanoparticles from Pulsed laser ablation (PLA) method with lanthanide ion doped inorganic phosphor as target is useful to various applications. Amans, et al. (2011) prepared nanoparticles using laser ablation (having laser pulse energy between  $\sim 2-70$  mJ) of doped oxides such as, Eu:Y<sub>2</sub>O<sub>3</sub>, Eu:Gd<sub>2</sub>O<sub>3</sub> and Ce:YAG in aqueous solution of 2-[2-(2-methoxyethoxy) ethoxy] acetic acid (MEEAA). The size and number of particles is controlled by varying laser pulse energy and solvent. Moreover,  $Er^{3+}/Yb^{3+}$  co-doped up-conversion materials have great ability to improve the solar cell efficiency. The enhancement of solar cell efficiency using up and down conversion Ln<sup>3+</sup> has been reported [Etchart, et al. (2010), Chen, et al. (2012), Ende, et al. (2009)].

Herein, we have prepared Y<sub>2</sub>Ti<sub>2</sub>O<sub>7</sub> (YTO) and Er<sub>x</sub>Yb<sub>y</sub>Y<sub>2-x-y</sub>Ti<sub>2</sub>O<sub>7</sub> (EYYTO) system through conventional solid state route and studied structural and optical properties of EYYTO. In particular, we illustrate an interesting approach to understand the mechanism of energy transfer from EYYTO (sensitizer) host to the dopants (activator) by incorporating the rare-earth ions ( $Er^{3+}$ ,  $Yb^{3+}$ ) which have unique charge-transfer associated excited states in their host (YTO or EYYTO) matrices. Laser power dependence on up-conversion luminescence has explained energy transfer mechanism between the absorbing host and the rare-earth emitters. Further, we have prepared the mono-dispersed colloidal solution of EYYTO employing laser ablation method and studied its emission and absorption spectra.

## 3.2 Experimental

### 3.2.1 Synthesis

Y<sub>2</sub>Ti<sub>2</sub>O<sub>7</sub> (YTO) and Er<sub>x</sub>Yb<sub>y</sub>Y<sub>2-x-y</sub>Ti<sub>2</sub>O<sub>7</sub> (x = 1 and y = 2 at. %) (EYYTO) samples were prepared by conventional solid state route. The starting materials used in the synthesis process were Y<sub>2</sub>O<sub>3</sub> (99.99%, Alfa Aesar), TiO<sub>2</sub> (99.9%, Alfa Aesar), Yb<sub>2</sub>O<sub>3</sub> (99.98%, Alfa Aesar) and Er<sub>2</sub>O<sub>3</sub> (99.9 %). For typical synthesis of Er<sub>x</sub>Yb<sub>y</sub>Y<sub>2-x-y</sub> Ti<sub>2</sub>O<sub>7</sub> (x = 1 and y

= 2 at. %) phosphor, the stoichiometric composition of these were mixed in a ball mill agate mortar at the speed of 50 rpm for three hours using acetone as a mixing medium. This mixed system was transferred into an alumina crucible and heated to 1200 °C in ambient atmosphere at the rate of 2 °C/min for 6 h. This was allowed to cool at room temperature by natural process. The mixture was ground using pestle mortar for 1 h; and pellets of 10 mm in diameter and 2 mm in thickness were prepared. The pellets were sintered at 1300 °C for 12 h. Similar process was adopted to prepare YTO sample. These samples were used further for the structural and optical characterizations.

### 3.2.2 Preparation of colloidal nanoparticles

Colloidal solution of the EYYTO powder was prepared via liquid pulsed laser ablation method. The pellet of the EYYTO powder was immersed in the distilled water medium and the laser light with wavelength 355 nm (with pulse repetition rate 10 Hz, pulse width 6 ns and pulse energy ~ 80 m J) was incident on the pellet. The laser beam was focussed by a convergent lens with 15 cm focal length. The pellet was immersed in water nearly 5 mm underneath the air-water interface. The pellet was rotated and the spot size of laser beam at the target surface was varied as ~1-2 mm in diameter by adjusting the distance between focusing lens and target of the sample during the process of ablation.

### 3.2.3 Characterization

X-ray diffraction (XRD) pattern was measured with a Rigaku miniflex-II diffractometer using  $CuK_{\alpha}$  radiation (1.5404 Å) at 30 kV and 15 mA in the range  $10 \leq 2\theta^{\circ} \leq 90^{\circ}$  with a step size of  $\Delta 2\theta = 0.02^{\circ}$ . Fourier transform infrared (FTIR) spectrum of the sample was recorded using Shimadzu spectrophotometer in the range from 600 - 400  $cm^{-1}$ . The small amount of sample was mixed with KBr (Sigma Aldrich, 99.99%) in 1:5 ratios and transparent pellet was prepared. The Raman spectra of the YTO and EYYTO were measured with Renishaw micro-Raman spectrometer attached with 514.5 nm  $Ar^{+}$  laser as an excitation source. The photoluminescence (PL) spectra were recorded using iHR320 (Horiba Jobin Yvon) spectrometer equipped with R928P photon counting photomultiplier tube and a 976 nm diode laser with 2.4 W maximum power as an excitation source. The PL decay measurement for  ${}^4S_{3/2} \rightarrow {}^4I_{15/2}$  transitions of  $Er^{3+}$  ion at 548 nm band was carried out with Jobin-Yvon spectro-fluorometer (Fluoromax-4P) at room temperature. This sample was excited with pulsed light source (UV-Xenon flash tube) and emission was monitored by monochromator attached with R928P photon counting detector. The life time decay

measurement was recorded at room temperature with  $\sim 976$  nm diode source. The luminescence signal was interfaced to a 150- MHz digital oscilloscope (model no. HM 1507, Hameg Instruments). The decay time was determined using the method of non-linear square fit. The goodness of fit was judged on the basis of  $R^2$  value with method of non-linear square fit. The absorption spectrum of the sample was recorded by UV-Vis Perkin Elmer Lambda-35 spectrophotometer. The microstructure analysis was carried out by transmission electron microscope (TEM) employing TECNAI 20 G<sup>2</sup> operated at an accelerated voltage of 200 kV. A 355 nm radiation (third harmonic) from a pulsed Nd-YAG laser (Spitlight 600, Innolas, Germany) was used to prepare the colloidal solution nanoparticles.

### 3.3 Results and discussion

#### 3.3.1 Structural analysis

##### 3.3.1.1 XRD study

Figure 3.1 shows the XRD patterns of YTO and EYYTO samples along with corresponding ( $hkl$ ) planes. All the peaks are well matched with JCPDS card no. 42-0413. It clearly shows that samples are well crystalline with face centered cubic lattice structure [Brixner (1964)].

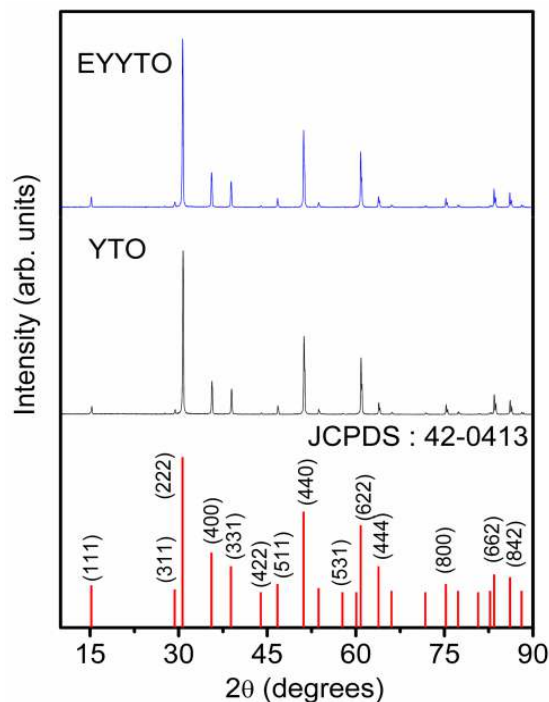


**Figure 3.1:** XRD patterns of  $\text{Y}_2\text{Ti}_2\text{O}_7$  (YTO) and  $\text{Er}^{3+}/\text{Yb}^{3+}$  doped  $\text{Y}_2\text{Ti}_2\text{O}_7$  (EYYTO) phosphor.

The average crystallite size of the sample were calculated using the Scherrer's formula,

$$D = \frac{k\lambda}{\beta_{hkl}\text{Cos}(\theta)} \quad (3.1)$$

where  $k = 0.89$ ,  $D$  average crystallite size,  $\lambda$  wavelength of  $\text{CuK}\alpha$ ,  $\theta$  Bragg's diffraction angle of the planes and  $\beta_{hkl}$  the corrected full width at half maximum (*FWHM*). For  $\beta_{hkl}$  correction,  $\beta_{inst}$  (*FWHM* due to instrument) is removed using *Si* standard [Cullity (1959), Parchur, et al. (2011b)]. The average crystallite size of YTO and EYYTO samples was found to be  $\sim 87$  and  $85$  nm, respectively. The structure refinement of the samples was carried out by using *FullProf* software [Carvajal J. R.]. The peak profiles were modelled using Pseudo-Voigt function and background was described in terms of a six coefficient polynomial. The  $R_{wp}$  (weighted-pattern factor) and  $S$  (goodness-of-fit) parameters were used as numerical criterion of the quality of fit of calculated to experimental diffraction data. Figures 3.2 (a) and (b) show the Rietveld refinement of powder diffraction data of YTO and EYYTO samples. The Bragg reflections, difference in observed and calculated intensity are also shown in the figure itself. The fitting parameters obtained after refinement are listed in Table 3.1. It is found that the unit cell volume slightly decreases after  $\text{Er}^{3+}/\text{Yb}^{3+}$  doping in YTO. This may be due to small ionic radius of  $\text{Er}^{3+}/\text{Yb}^{3+}$  ions as compared to  $\text{Y}^{3+}$  ion [Shanon (1976)].

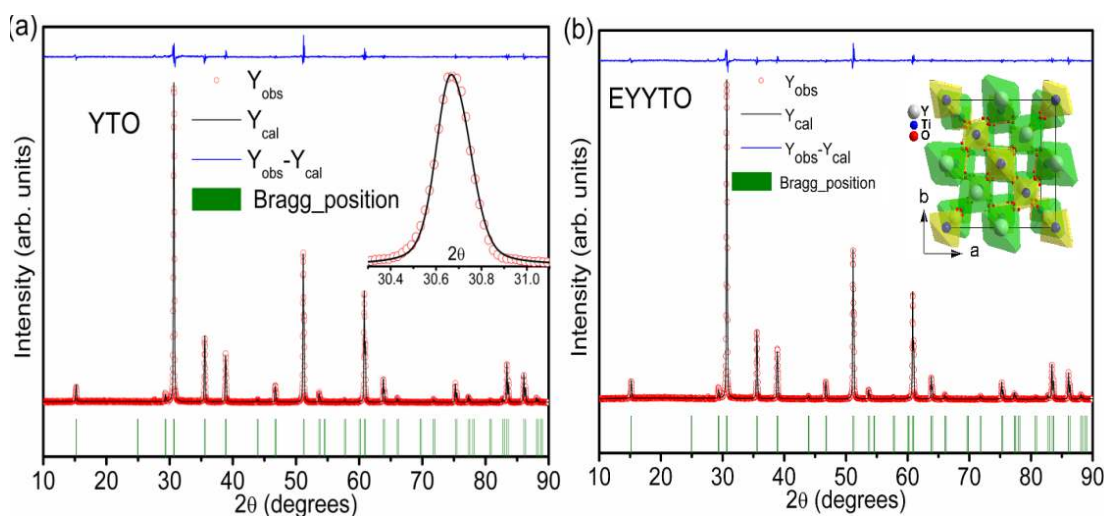


**Figure 3.2:** Rietveld refinements for X-ray diffraction data of (a)  $\text{Y}_2\text{Ti}_2\text{O}_7$  (YTO) and (b) 1 at.%  $\text{Er}^{3+}$  and 2 at.%  $\text{Yb}^{3+}$  doped  $\text{Y}_2\text{Ti}_2\text{O}_7$  (EYYTO). Calculated positions of Bragg reflections are shown by vertical tick marks (bottom) and top row shows the difference in observed and calculated diffraction peak intensity. Inset of (a) shows the expansion of typical Rietveld fitting to experimental data between  $30.4$  to  $31.1^\circ$ . Inset of (b) shows the polyhedral representation of  $\text{Y}_2\text{Ti}_2\text{O}_7$ .

The diffraction patterns intensity of EYYTO was found to be slightly less than YTO samples which may be due to defects created in  $Er^{3+}/Yb^{3+}$  doped YTO.

**Table 3.1:** Parameters obtained after refinement of observed XRD data.

Parameters	Compositions	
	$Y_2Ti_2O_7$ (YTO)	$Y_2Ti_2O_7:Er^{3+}/Yb^{3+}$ (EYYTO)
Y(x, y, z)	(0.5, 0.5, 0.5)	(0.5, 0.5, 0.5)
Ti(x, y, z)	(0, 0, 0)	(0, 0, 0)
O <sub>1</sub> (x, y, z)	(0.324, 0.125, 0.125)	(0.323(4), 0.125, 0.125)
O <sub>2</sub> (x, y, z)	(0.375, 0.375, 0.375)	(0.375, 0.375, 0.375)
Angles( $\alpha$ , $\beta$ , $\gamma$ )	( 90, 90, 90)	( 90, 90, 90)
Lattice Parameters (a)	10.095	10.095
Unit Cell Volume $\text{\AA}^3$	1028.92	1028.64
$\chi^2$	4.71	3.91
Y-O <sub>1</sub>	2.519	2.5124
Y-O <sub>2</sub>	2.1857	2.1855
Ti-O <sub>1</sub>	1.9342	1.9377
$R_{wp}$	17.6	16.1
$R_p$	15.7	15.5

Inset in Figure 3.2 (a) shows the expansion of typical Rietveld fitting to the experimental data of (222) plane between 30.4 to 31.1° and the three dimensional polyhedral representation of EYYTO sample is shown in inset of Figure 3.2 (b). In  $Y_2Ti_2O_7$  pyrochlore, the larger cations sit at *A* site (16c) with 8 coordination number while the smaller one sits at *B* site (16d) with 6 coordination. The oxygen atoms occupy the three different crystallographic axes as 48f (O<sub>1</sub>), 8a (O<sub>2</sub>) and 8b (O<sub>3</sub>). In  $Y_2Ti_2O_7$ , 48f (O<sub>1</sub>) site is



tetrahedrally coordinated to two Ti and two Y cations while 8a ( $\text{O}_2$ ) is linked with four Y cations, respectively. The third anionic site in the unit cell is 8b ( $\text{O}_3$ ) which is tetrahedrally coordinated with four Ti cations and generally found to be empty for perfectly ordered pyrochlore [Sanjuan, et al. (2011)].

### 3.3.1.2 TEM study

TEM images of EYYTO phosphor and its laser ablated colloidal solution are shown in Figure 3.3 (a) and (c) along with corresponding selected area electron diffraction (SAED) patterns in Figures 3.3 (b) and (d), respectively. An irregular spherical microsphere is observed. The SAED analysis was performed to confirm the crystallinity of the prepared material. The result of SAED patterns reveals corresponding ( $hkl$ ) planes. The average particle size in colloidal solution was found to be  $\sim 100$  nm.

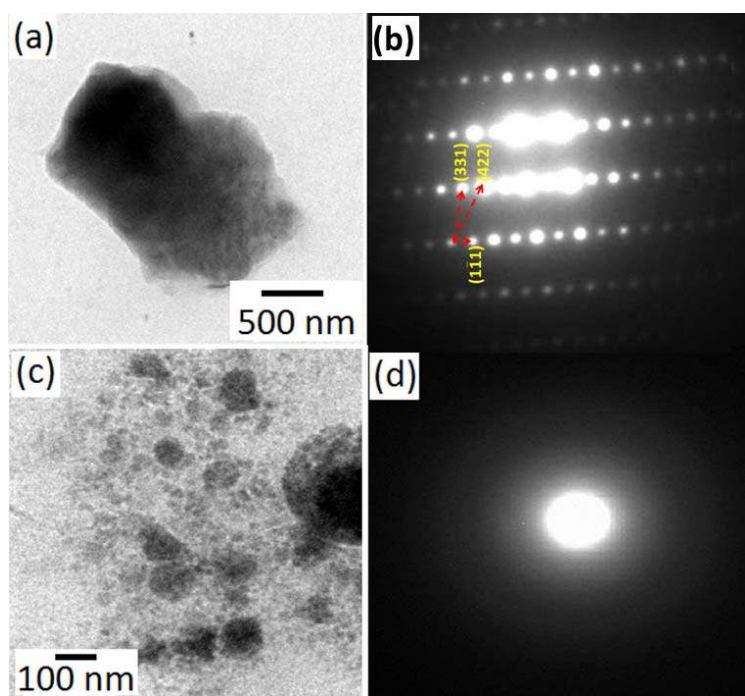


**Figure 3.3:** TEM images of (a)  $\text{Er}^{3+}/\text{Yb}^{3+}$  doped  $\text{Y}_2\text{Ti}_2\text{O}_7$ , (c) colloidal solution. Their corresponding SAED patterns are shown in (b) and (d), respectively.

### 3.3.1.3 FTIR study

FTIR spectrum of EYYTO is shown in Figure 3.4. The absorption bands appeared at  $\sim 417$ ,  $436$ ,  $484$ ,  $494$  and  $573$   $\text{cm}^{-1}$  are related to  $\text{Y-O}_1$ ,  $\text{Y-O}_2$  and  $\text{Ti-O}$ , stretching vibrations [Gill, et al. (2012)]. The band around  $500$  and  $400$   $\text{cm}^{-1}$  are assigned to  $\text{Y-O}_1$  and  $\text{Y-O}_2$  stretching vibrations in the  $\text{Y}_2\text{Ti}_2(\text{O}_1)_6\text{O}_2$  polyhedron of  $\text{Y}_2\text{Ti}_2\text{O}_7$ . It was found that the absorption bands of YTO sample at  $573$ ,  $473$  and  $417$   $\text{cm}^{-1}$  which are assigned to  $\text{Ti-O}$ ,



Y-O<sub>2</sub> and Y-O<sub>1</sub> stretching vibrations, respectively [Chen, et al.(2011)]. These are the main features of the titanate pyrochlore IR-spectra. These vibrations confirm the formation of Y<sub>2</sub>Ti<sub>2</sub>O<sub>7</sub> structure.

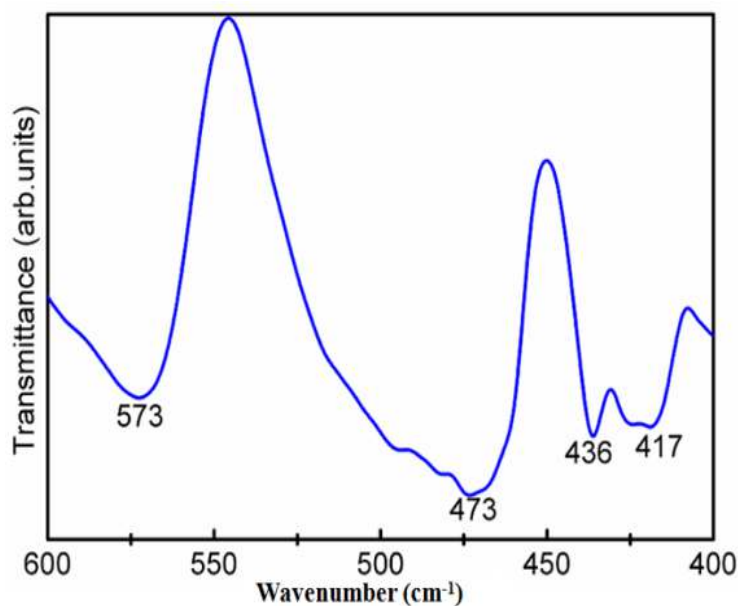


**Figure 3.4:** FTIR spectrum of  $Er^{3+}/Yb^{3+}$  doped  $Y_2Ti_2O_7$  (EYYTO) phosphor.

### 3.3.1.4 Raman study

The Raman spectra of pure YTO and EYYTO samples are shown in the Figure 3.5(a) and (b). Since the pyrochlore ( $A_2B_2O_7$ ) is a superstructure of fluorite formed by ordering of A and B cations into uneven crystallographic sites and ordering of anions into three sites 48f ( $O_1$ ), 8a ( $O_2$ ) and 8b ( $O_3$ ). Therefore, Raman spectroscopy provides the degree of disorder in pyrochlore and hence distinguishes between defects pyrochlore to fluorite structures. Raman spectroscopy is more sensitive to metal-oxygen vibrational modes in comparison to metal-metal vibrational modes. There are six Raman active modes are found in  $A_2B_2O_7$  pyrochlores having space group ( $Fd\bar{3}m$ ,  $Z=8$ ). These modes arise due to vibration of oxygen at 48f ( $O_1$ ) and 8a ( $O_2$ ). A and B cations do not contribute to active Raman bands because they possess centrosymmetric symmetry with inversion centre. At room temperature pure YTO shows the well known Raman bands of at  $\sim 212$ , 307, 515, and 710  $cm^{-1}$  and very weak band near 800  $cm^{-1}$ . The active Raman bands in this compound to  $\Gamma_{Raman} = A_{1g} + E_g + 4T_{2g}$ , the symbols represent the irreducible group representation [Sanjuan, et al. (2011)]. Gupta and Brown (2003) calculated the active IR and the Raman bands for YTO sample and explained that the numbers of IR and Raman active modes for this system are seven and six, respectively.

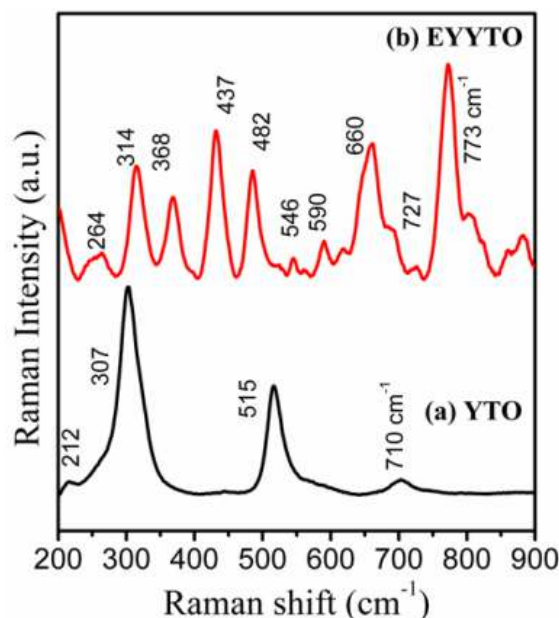


**Figure 3.5:** Raman spectra of (a) YTO and (b) EYYTO samples recorded at room temperature.

The active Raman bands were  $A_{1g}$ ,  $E_g$  and  $4T_{2g}$  while IR active is  $7F_{1u}$ . Sanjuan, et al. (2011) explained the characteristic modes of YTO pyrochlore observed at  $\sim 310 \text{ cm}^{-1}$  which has the contributions from  $E_g$  and  $T_{2g}$  modes both. The bands at  $\sim 515 \text{ cm}^{-1}$  and  $711 \text{ cm}^{-1}$  correspond to  $A_{1g}$  mode of vibration and one of the  $T_{2g}$  mode of vibration, respectively. The  $A_{1g}$  frequency mode fetches the information about the force constant of YTO pyrochlore. The vibration of the  $\text{TiO}_6$  octahedra is responsible for the  $A_{1g}$  mode of vibration of YTO pyrochlore structure. The major contribution for this mode is mainly due to the force constants associated with O-Ti-O bending [Brown, et al. (2003)]. Vanderborre, et al. (1983) explained the Raman spectra of different stannates and titanates for the higher frequency  $T_{2g}$  modes of vibrations. These higher  $T_{2g}$  modes of vibrations occur due to the force constant of Ti-O bond in  $\text{TiO}_6$  octahedra. Recently, Camacho, et al. (2012) studied the Raman spectra of  $\text{Er}^{3+}/\text{Yb}^{3+}$  doped hybrid materials and reported that the band situated near  $\sim 368 \text{ cm}^{-1}$  is the metal oxygen (Yb-O) similar to the band at  $377 \text{ cm}^{-1}$  of (Y-O) stretching vibration, while characteristic peaks of  $\text{Er}^{3+}$  ion are found in the range of  $\sim 500\text{-}580 \text{ cm}^{-1}$  and also some small traces of Raman bands near  $\sim 620\text{-}680 \text{ cm}^{-1}$  and  $\sim 780\text{-}900 \text{ cm}^{-1}$  are observed. Some additional Raman modes with lower intensities are also observed due to local disorder and defects present in the pyrochlore lattice of EYYTO. Radhakrishnan, et al. (2011) described the presence of local disordering and defects in Ca and Mo substituted  $\text{Gd}_2\text{Ti}_2\text{O}_7$ . They reported that disordering and defects present in the system distort the translational periodic arrangement of the lattice and hence allows the  $k = 0$  selection rule,

which is the main cause of the occurrence of additional Raman bands with lower intensities in the EYYTO pyrochlore structure.

### 3.3.2 Optical Characterizations

#### 3.3.2.1 Up-conversion and pump power dependence study

Up-conversion (UC) is a nonlinear optical phenomenon in which light of higher wavelength near infrared or infrared (i.e. NIR or IR) is converted into visible or UV (ultraviolet) light through multiphoton absorption and energy transfer (ET) processes [Auzel (2004)]. On excitation with 976 nm laser, large number of bands starting from UV to Vis to NIR could be observed due to  $\text{Er}^{3+}$  ions. The bands appearing in green and red regions are very intense and lie in the anti-stoke side of the pump beam. These bands are shown in Figure 3.6.

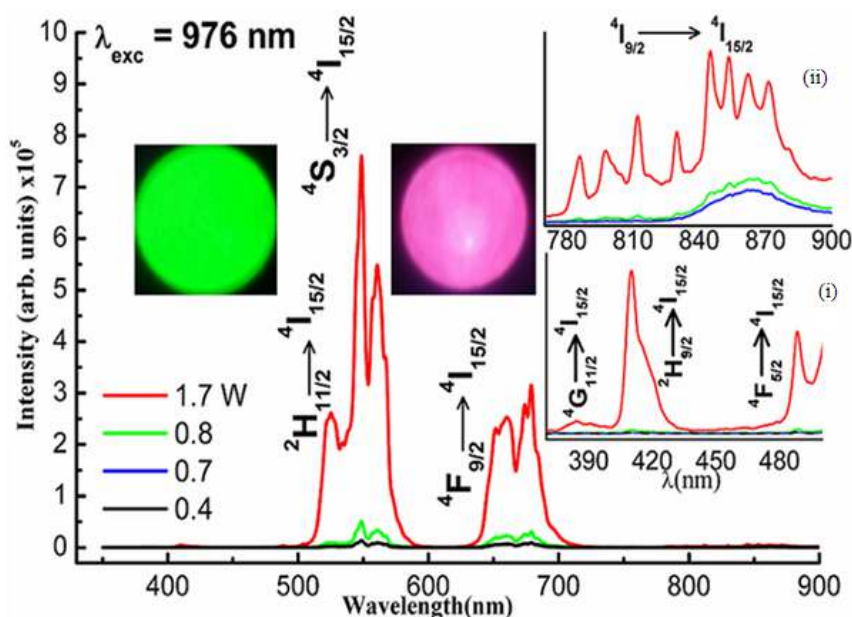


**Figure 3.6:** Emission spectra of  $\text{Er}^{3+}/\text{Yb}^{3+}$  doped  $\text{Y}_2\text{Ti}_2\text{O}_7$  phosphor under 976 nm excitation wavelengths at different pump power (up-conversion). Inset shows the expansion from 370-500 nm (bottom) and 775-900 nm (top). Digital photograph of the sample using green and red colour filters are shown in Inset.

In order to understand the UC mechanism involved in the EYYTO system, we have analysed the pump power dependence of up-conversion fluorescence intensity. Emission spectra of EYYTO sample were recorded with ~0.4, 0.7, 0.8 and 1.7 W laser input power in the range of 350- 900 nm. Two prominent bands are observed due to up-conversion at ~524, 548 nm which are responsible for green emission situated in between 500- 600 nm with maximum intensity at ~548 nm. These two bands arise due to  ${}^2\text{H}_{11/2} \rightarrow {}^4\text{I}_{15/2}$ , and  ${}^4\text{S}_{3/2}$

→<sup>4</sup>I<sub>15/2</sub> electronic transitions, respectively of the Er<sup>3+</sup> ion. Also the band observed in the range 600 to 700 nm with maximum intensity at ~661 nm was assigned to <sup>4</sup>F<sub>9/2</sub> →<sup>4</sup>I<sub>15/2</sub> transition. Moreover, peaks at ~380, 410 and 487 nm in near UV and blue region of the spectrum with low intensity which is well described in the inset (i) from 380-500 nm. These bands arise due to the electronic transitions namely, from <sup>4</sup>G<sub>11/2</sub> →<sup>4</sup>I<sub>15/2</sub>, <sup>2</sup>H<sub>9/2</sub> →<sup>4</sup>I<sub>15/2</sub> and <sup>4</sup>F<sub>5/2</sub> →<sup>4</sup>I<sub>15/2</sub> of Er<sup>3+</sup> ion on 976 nm excitation. Inset (ii) ranging from 750-900 nm, which are splitted Stark pattern of <sup>4</sup>I<sub>9/2</sub> →<sup>4</sup>I<sub>15/2</sub> of Er<sup>3+</sup> ion. The Stark splitting clearly demonstrate the highly crystalline nature of EYYTO phosphor. It is also observed that stark splitting of the transition is less in low excitation power and become clear with increasing power. The stark splitting patterns also suggest that Er<sup>3+</sup> ions are situated in well located crystallite sites of face centered cubic pyrochlore [Chen, et al.(2011)]. The levels are populated partially by direct absorption and partly through energy transfer from Yb<sup>3+</sup> to Er<sup>3+</sup> ions. Since, Er<sup>3+</sup> has poor absorption cross section ( $1.7 \times 10^{-21} \text{ cm}^2$ ) than its Yb<sup>3+</sup> counterpart, which has very high absorption cross section ( $11.7 \times 10^{-21} \text{ cm}^2$ ) at 976 nm excitation [Strohhofer and Polman (2003)]. Generally, there are two possible processes namely, excited state absorption (ESA) and energy transfer (ET) up-conversion, responsible for up-conversion emission. In context of ESA process, the green and red emissions arising from Er<sup>3+</sup> ion can be explained on the basis of these two mechanisms, which are resulting on excitation at 976 nm. The Er<sup>3+</sup> ion in its ground state absorbs the incident photons and promoted to <sup>4</sup>I<sub>11/2</sub> excited state, whereas the absorption of next photons of same energy Er<sup>3+</sup> ions are promoted to the <sup>4</sup>F<sub>7/2</sub> level. The ions in <sup>4</sup>F<sub>7/2</sub> level decays through nonradiative channel via multi phonon process to <sup>2</sup>H<sub>11/2</sub> and <sup>4</sup>S<sub>3/2</sub> levels. In the ET process, there is probability of two Er<sup>3+</sup> ions excited to their <sup>4</sup>I<sub>11/2</sub> state via GSA or one Er<sup>3+</sup> ion is promoted in <sup>4</sup>I<sub>11/2</sub> level (GSA) and one Yb<sup>3+</sup> ion in the <sup>2</sup>F<sub>5/2</sub> level (GSA). The Yb<sup>3+</sup> ion transfers its energy to Er<sup>3+</sup> to excite it to <sup>4</sup>I<sub>11/2</sub> level. The two excited Er<sup>3+</sup> ions in the <sup>4</sup>I<sub>11/2</sub> level exchange their energy and one decays to the ground state <sup>4</sup>I<sub>15/2</sub> and the other is promoted to <sup>4</sup>F<sub>7/2</sub> level. The ion in <sup>4</sup>F<sub>7/2</sub> level, via non-radiative relaxation reaches to <sup>2</sup>H<sub>11/2</sub> and <sup>4</sup>S<sub>3/2</sub> levels. The <sup>2</sup>H<sub>11/2</sub> and <sup>4</sup>S<sub>3/2</sub> levels are populated via ET and ESA processes. The resulting green emissions at lower levels are due to these <sup>2</sup>H<sub>11/2</sub> →<sup>4</sup>I<sub>15/2</sub> and <sup>4</sup>S<sub>3/2</sub> →<sup>4</sup>I<sub>15/2</sub> energy level transitions. The involved transitions of different emitting levels in the up-conversion process via ET and ESA along with GSA are schematically shown in the Figure 3.7.

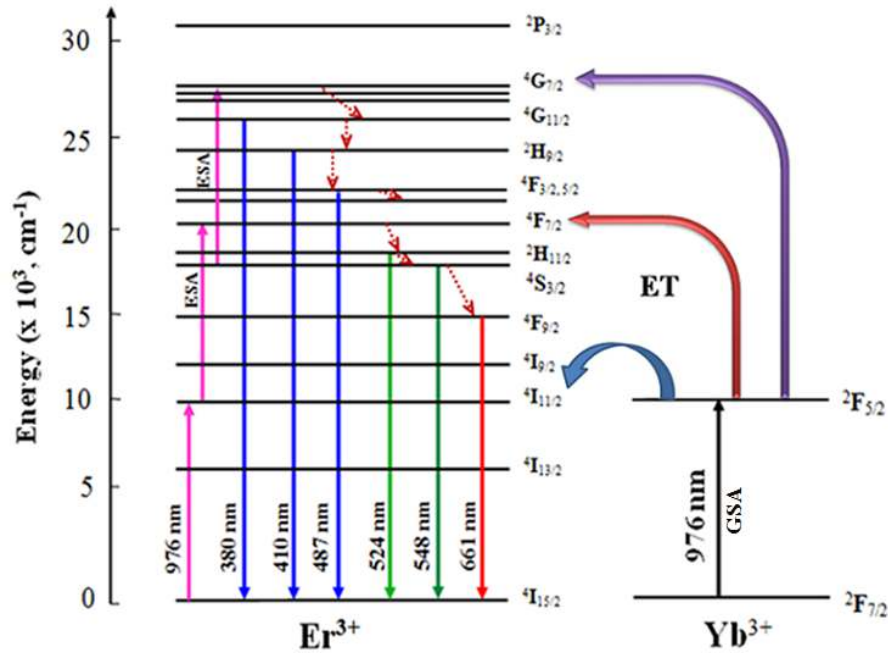
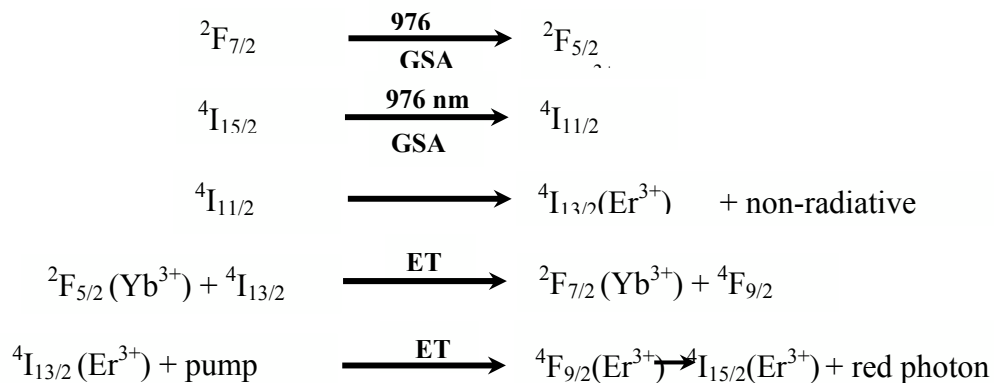


**Figure 3.7:** Energy level diagram of Er<sup>3+</sup> and Yb<sup>3+</sup> ions with proposed up-conversion mechanism under 976 nm laser excitation.

Also part of the ion in <sup>4</sup>S<sub>3/2</sub> can further relax and populate the <sup>4</sup>F<sub>9/2</sub> level leading to the <sup>4</sup>F<sub>9/2</sub> → <sup>4</sup>I<sub>15/2</sub> transition (red emission). The <sup>4</sup>F<sub>9/2</sub> level may also be populated from the <sup>4</sup>I<sub>13/2</sub> level of the Er<sup>3+</sup> ion by absorption of a 976 nm photon, or by energy transfer from Yb<sup>3+</sup> ion. The <sup>4</sup>I<sub>13/2</sub> state is initially populated via the non-radiative <sup>4</sup>I<sub>11/2</sub> → <sup>4</sup>I<sub>13/2</sub> relaxation [Ferrari, et al. (2012)]. As the energy gap between the <sup>4</sup>S<sub>3/2</sub> to <sup>4</sup>F<sub>9/2</sub> is quite large (~3000 cm<sup>-1</sup>), the probability of nonradiative relaxation is smaller while the second channel seems to contribute more effectively. A bright green up-converted light is emitted through <sup>4</sup>S<sub>3/2</sub> + <sup>2</sup>H<sub>11/2</sub> → <sup>4</sup>I<sub>15/2</sub> while comparatively weak red emission is observed from <sup>4</sup>F<sub>9/2</sub> → <sup>4</sup>I<sub>15/2</sub> levels [Kumar, et al. (2012), Manzani, et al.(2012)]. The involved mechanism in red band emission is as follows;



So, the involvement of two photons is observed for the green ( $\sim 524$  and  $\sim 548$  nm) and red bands ( $\sim 661$ nm) emission, which is well supported by the  $n$  value obtained for these bands from Figure 3.8 (a). Similarly, the up-conversion mechanism channel can be explained for UV and visible bands i.e. for  $\sim 380$ , 410 and 487 nm and the involvement of three photons is observed for these bands which is shown in Figure 3.8 (b). As  $\text{Er}^{3+}$  and  $\text{Yb}^{3+}$  ions irradiated with 976 nm radiation and promoted to their excited states (GSA). Since, the absorption cross section of sensitizer ( $\text{Yb}^{3+}$ ) is very much high in comparison to ( $\text{Er}^{3+}$ ), therefore most of the photons were absorbed by ( $\text{Yb}^{3+}$ ) ions and transfers its energy to ( $\text{Er}^{3+}$ ) ions via ET pathways. The absorption of second photon in excited state promotes the  $\text{Er}^{3+}$  ions to  $^4\text{F}_{7/2}$  and  $^4\text{S}_{3/2}$  levels. A subsequent absorption of third photon promoted the  $\text{Er}^{3+}$  ion to its  $^4\text{G}_{7/2}$  levels. To understand the up-conversion influence of the observed luminescence, we have studied the intensity of the band with respect to pump power. The integrated band intensities near UV and Visible region in variance with a function of laser excitation power which is shown in the Figure 3.8. In the up-conversion mechanism, the emission intensities follow the relation as  $I \propto P^n$ , where  $I$  is the up-conversion intensity,  $P$  is the pump power;  $n$  is the number of NIR photons involved in the up-conversion [Pandozzi, et al. (2005)]. Number of photons  $n$  is obtained from slope of the straight line by fitting the bi-logarithmic plot of pump power versus emitted intensity.  $n$  values obtained for 524, 548 and 661 nm bands are shown in Figure 3.8 (a) and Value of  $n$  obtained for  $\sim 380$ ,  $\sim 410$  and  $\sim 487$  nm as shown in Figure 3.8 (b) itself.

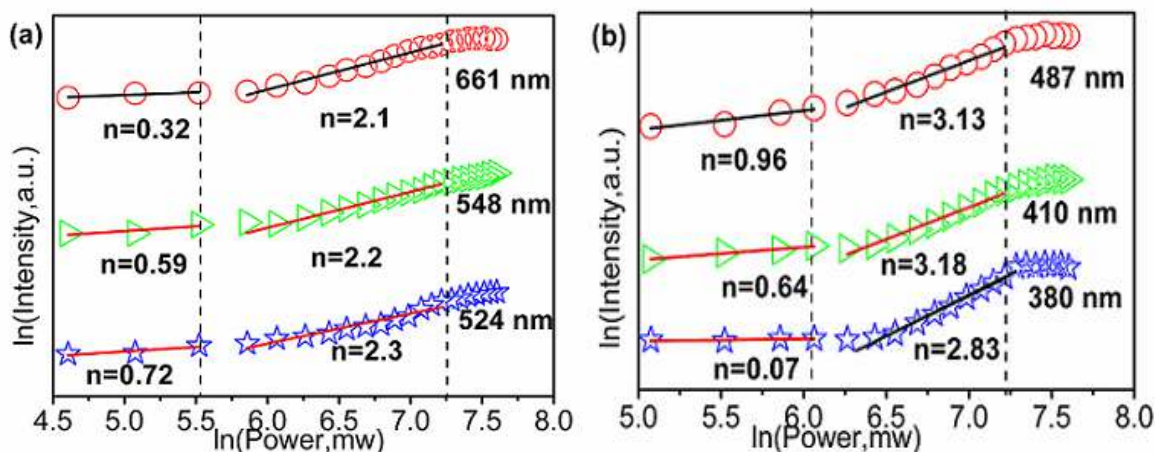


**Figure 3.8:** Power dependence of (a) visible (524, 548 and 661 nm) and (b) UV, blue 380, 410 and 487 nm) bands.



Pollnau, et al.(2000) proposed the model on the power dependence behaviour of luminescence intensity and explain the slope value for different powers by solving the rate equations and reported that up-conversion rate enhances for the moderate power but for higher value of pump power it becomes almost constant. From the power dependence study, quadratic behaviour is observed for green and red bands while for ultraviolet and blue bands, involvement of three photons was observed. The characteristics emission intensities of green band over red one is quite different from the earlier reported one. Enhancement in photoluminescence intensity was observed even at lower at% of  $\text{Er}^{3+}$  and  $\text{Yb}^{3+}$  concentration which demonstrate the color tunability of the host material. Chen et al.(2011) have reported the up-conversion behaviour of  $\text{Er}^{3+}/\text{Yb}^{3+}$  doped YTO with varying  $\text{Yb}^{3+}$  concentration and observed the intense red emission. Recently, photoluminescence modification and energy transfer mechanism was reported by Yan, et al.(2012) for up-conversion behaviour of tri-doped ( $\text{Er}^{3+}/\text{Yb}^{3+}/\text{Tm}^{3+}$ )  $\text{Y}_2\text{Ti}_2\text{O}_7$  inverse opal. It was reported that the improvement in energy transfer occur between  $\text{Er}^{3+}$  and  $\text{Tm}^{3+}$  at 980 nm excitation. Thus the intensity variation observed for the green and red bands is mainly due to energy transfer from ( $\text{Yb}^{3+}$  to  $\text{Er}^{3+}$ ). The maximum up-conversion intensity is observed for 1 at.%  $\text{Er}^{3+}$  and 2 at.% of  $\text{Yb}^{3+}$  ions. For higher atomic percentage of  $\text{Er}^{3+}$ , cross relaxation (CR) becomes dominant process and the luminescence quenches [Dexter (1953)].

### 3.3.2.2 Variation of green- red ratio with input diode power

The variation of green to red intensity ratio as a function of excitation power is shown in the Figure 3.9.

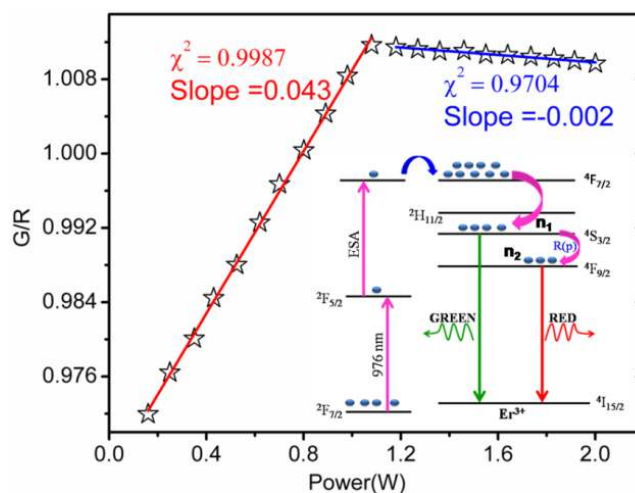


**Figure 3.9:** Variation of intensity of green ( ${}^4\text{S}_{3/2} \rightarrow {}^4\text{I}_{15/2}$ ) to red ( ${}^4\text{F}_{9/2} \rightarrow {}^4\text{I}_{15/2}$ ) band at different input laser powers of  $\text{Er}^{3+}/\text{Yb}^{3+}$  doped  $\text{Y}_2\text{Ti}_2\text{O}_7$  (EYYTO) phosphor. Inset shows the possible transitions for green and red emissions.



This ratio increases as a function of the excitation power up to  $\sim 1.0$  W revealing that green emission is dominant over red one. As far as the higher excitation powers i.e. at  $\sim 1.2$  to  $2.4$  W, again green emission becomes dominant over the red one. In order to have an idea about variation of the green to red ratio, we normalized the intensity of  $\sim 548$  nm band and compared its intensity with the intensities of  $\sim 524$  and  $661$  nm bands at the same pump power. The detailed analyses of these band intensity variations with input diode powers are given in the Figure 3.10 (a) and (b) and (c). For the  $524$  nm band, the green to red intensity ratio shows an increasing behaviour from low to high power, while for  $661$  nm band, it is high for low power and decreasing for the high power indicating that green band dominates at higher power. This dominant emission is explained by the proposed model which is given in the inset figure. Since, the probability of decay rate is not the same for  $^4S_{3/2}$  and  $^4F_{9/2}$ , therefore the excitation power limit is not the same for the both states. In order to explain the observed green and red emission, let  $n_1$  and  $n_2$  be the no. of photons in the state  $^4F_{7/2}$  and  $^4F_{9/2}$ , respectively.

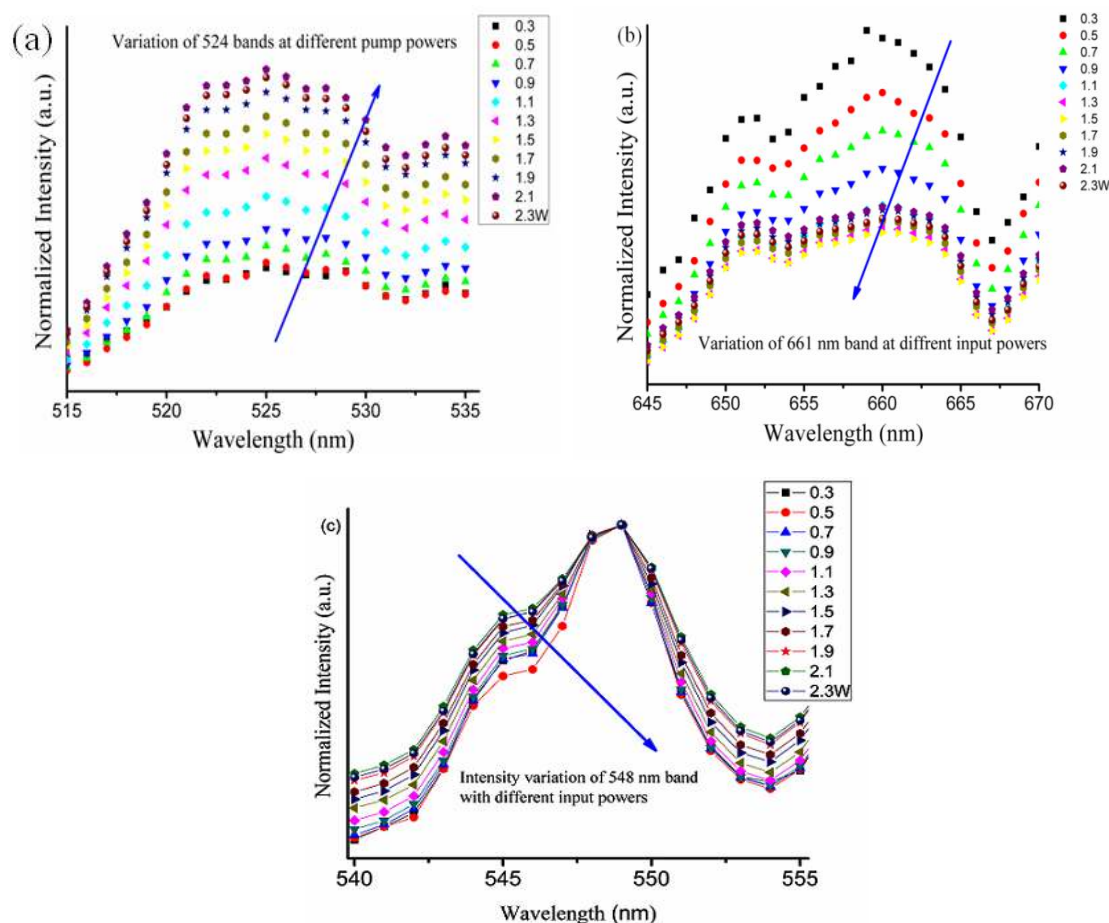


**Figure 3.10:** Variation in intensity with different input powers for (a) 524 and (b) 661 and (c) normalizing the emission intensity at 548 nm.

The decay rate  $R(p)$  as a function of power from  ${}^4\text{F}_{7/2}$  to  ${}^4\text{S}_{3/2}$  increases rapidly at the moderate power (up to  $\sim 1$  W) and  ${}^4\text{S}_{3/2}$  state populated and the electronic transition from  ${}^4\text{S}_{3/2} \rightarrow {}^4\text{I}_{15/2}$ , which gives the intense green emission. Since, the phonon vibration energy and heat generated at surface of the sample is enhanced as the power enhances to the higher value and hence the decay probability of photons (say  $n_2$ ) at  ${}^4\text{S}_{3/2}$  to  ${}^4\text{F}_{9/2}$  level increases slightly and electronic transition from  ${}^4\text{F}_{9/2} \rightarrow {}^4\text{I}_{15/2}$ , gives slightly improved red emission as clearly seen in the inset. Similar behaviour is reported in the literature for  $\text{Er}^{3+}/\text{Yb}^{3+}$  co-doped  $\text{SiO}_2$ - $\text{Ta}_2\text{O}_5$  glass ceramics by Ferrari, et al.(2012).

### 3.3.2.3 Colloidal solution study

The absorption and the emission spectra of the colloidal solution are shown in Figures 3.11 (a) and (b). The red emission bands show a very different intensity distribution under 976 nm excitation. In emission spectrum, red band shows variation in intensity distribution in comparison to green one.

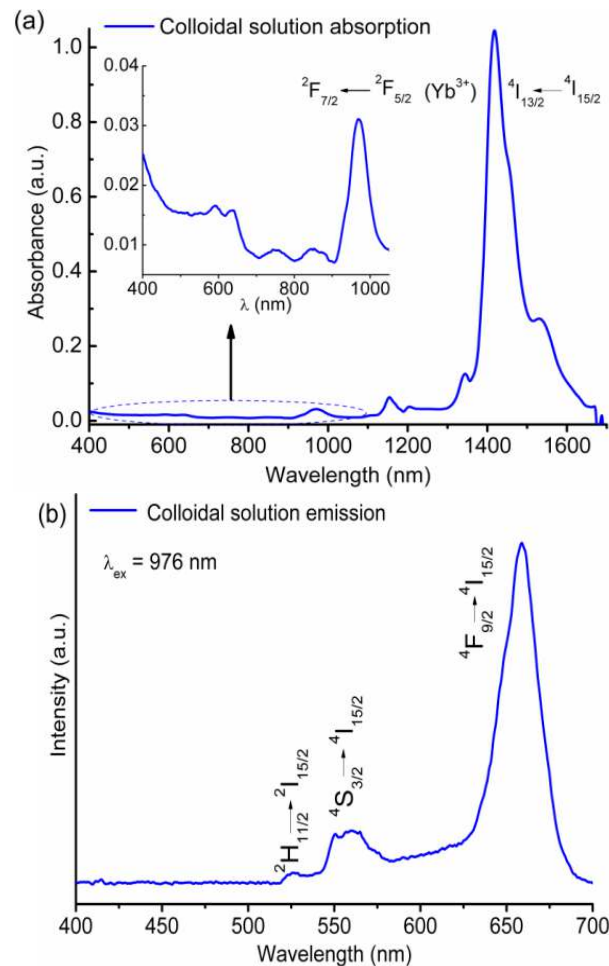


**Figure 3.11:** (a) Absorption spectrum (b) Up-conversion spectrum of  $\text{Er}^{3+}/\text{Yb}^{3+}$  doped  $\text{Y}_2\text{Ti}_2\text{O}_7$  (EYYTO) colloidal nanoparticles.

This explains that the excited ions relax rapidly to the lower excited level in colloidal solution. The absorption spectrum of colloidal solution prepared by laser ablation method show a strong absorption band at  $\sim 1440$  nm of  $\text{Er}^{3+}$  ion due to its  $^4\text{I}_{15/2} \rightarrow ^4\text{I}_{13/2}$  transition in  $\text{Er}^{3+}$ . Due to limitations with our instrumental facilities in NIR region, we have not been able to record the emission spectra over NIR range. A strong emission bands from the colloidal solution is observed at  $1.45 \mu\text{m}$ . It is also reported by Liu, et al.(2009) for  $\text{Er}^{3+}/\text{Yb}^{3+}$  doped  $\text{NaYF}_4$  nanocubes under  $976$  nm laser diode excitation and found the highest optical amplification gain for  $1.5 \mu\text{m}$ . The strong emission band occurs due to the efficient energy transfer from  $\text{Yb}^{3+}$  to  $\text{Er}^{3+}$  ion to give  $^4\text{I}_{13/2} \rightarrow ^4\text{I}_{15/2}$  transition. Though the absorption band due to  $\text{Yb}^{3+}$  have higher absorption cross section than its  $\text{Er}^{3+}$  ion, its band at  $\sim 976$  nm appears with weak intensity. The emission band at  $\sim 661$  nm in  $\text{Er}^{3+}$  appears with large intensity on excitation with  $976$  nm radiation. It seems that  $\text{Er}^{3+}$  ions in  $^4\text{I}_{13/2}$  level absorb  $976$  nm radiations and populated the  $^4\text{F}_{9/2}$  to give  $^4\text{F}_{9/2} \rightarrow ^4\text{I}_{15/2}$  transition emitting red photon.

### 3.3.2.4 Chromaticity of $\text{Er}^{3+}/\text{Yb}^{3+}:\text{Y}_2\text{Ti}_2\text{O}_7$ and color tuning

The CIE (*Commission Internationale de l'Eclairage*) system gives the parameters  $x$  and  $y$  to demonstrate the color perception. This includes the hue and saturation on a two dimensional chromaticity diagram. The color perception changes from low input diode pump power i.e. from  $\sim 0.3$  W to green to high power  $2.4$  W to give orangish red, which is demonstrated in terms of the CIE coordinates, calculated at the different powers.

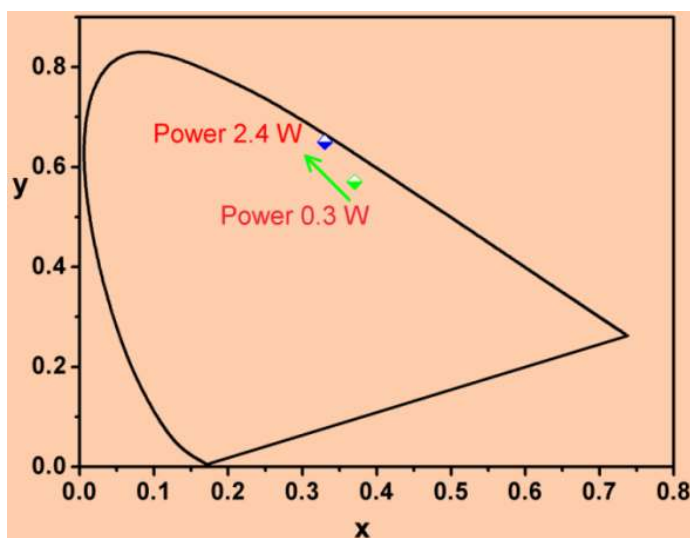


**Figure 3.12:** CIE chromaticity diagram at different laser input power showing the color tunability of  $\text{Er}^{3+}/\text{Yb}^{3+}$  doped  $\text{Y}_2\text{Ti}_2\text{O}_7$  (EYYTO) phosphor.

It is found that the color coordinates vary with pump power. Since up-conversion efficiency of rare earth doped YTO for different colors depend on the excitation power. In Figure 3.12, it is obvious that for low input power at  $\sim 0.3$  W, the color coordinates  $x, y$  are (0.37, 0.57) and for high input power (at  $\sim 2.4$  W), they are (0.33, 0.65).

The variation of CIE coordinates with different input diode powers are given in the Figure 3.13 and in table 3.2.

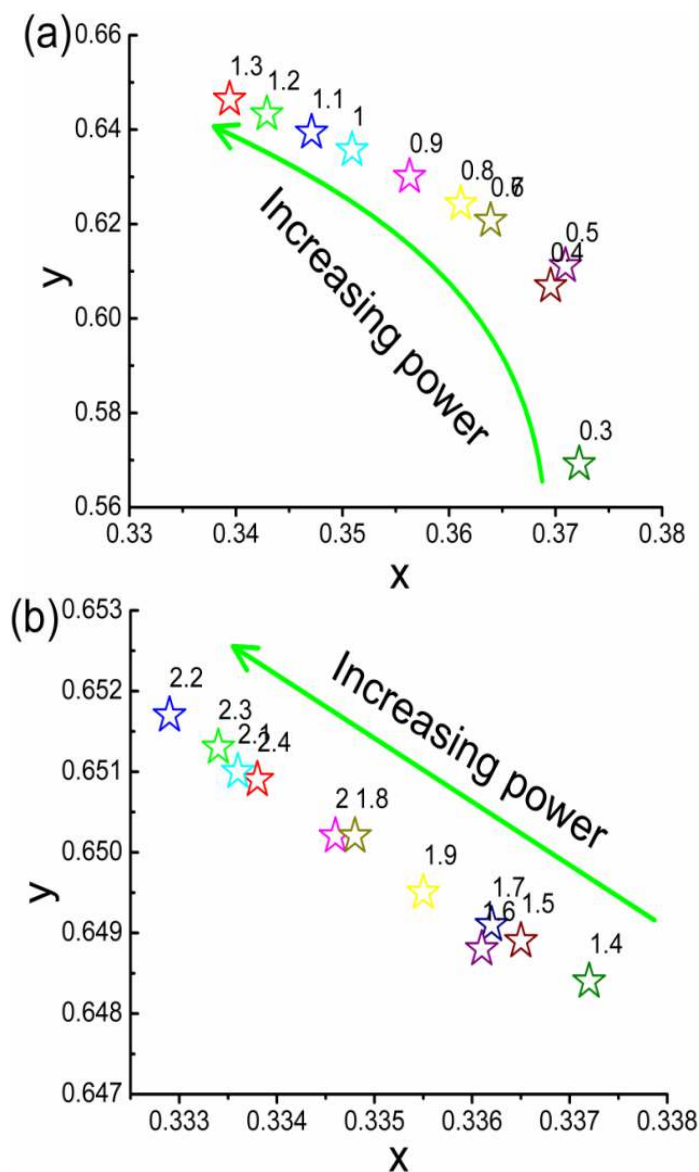


**Figure 3.13:** (a, b) show the variation of CIE coordinates with input laser power.

The variation of CIE coordinates with input laser power has been calculated and given in Table 3.2.

**Table 3.2:** CIE coordinates with input laser power.

Power (w)	x	y
0.3	0.372	0.569
0.4	0.370	0.607
0.5	0.371	0.611
0.6	0.364	0.621
0.7	0.364	0.621
0.8	0.361	0.624
0.9	0.356	0.630
1.0	0.351	0.636
1.1	0.347	0.639
1.2	0.343	0.643
1.3	0.339	0.646
1.4	0.337	0.648
1.5	0.337	0.649
1.6	0.336	0.649
1.7	0.336	0.649
1.8	0.335	0.650
1.9	0.336	0.650
2.0	0.335	0.650
2.1	0.334	0.651
2.2	0.333	0.652
2.3	0.333	0.651
2.4	0.334	0.651

### 3.3.2.5 Luminescence decay study

The lifetime decay profile of was recorded under 976 nm ( $\lambda_{\text{ex}}$ ) excitation by monitoring the emission of green band at  $\sim 548$  nm ( ${}^4\text{S}_{3/2} \rightarrow {}^4\text{I}_{15/2}$ ), is shown in Figure 3.14.

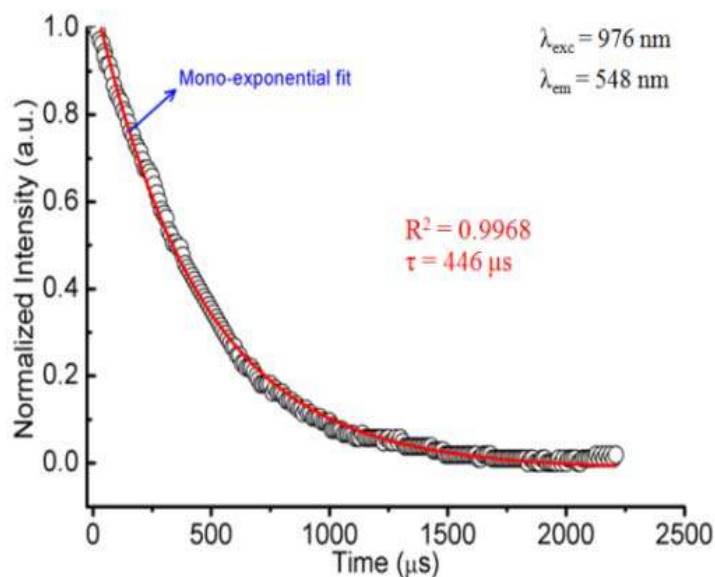


**Figure 3.14:** Luminescence decay curve of  $\text{Er}^{3+}/\text{Yb}^{3+}$  doped  $\text{Y}_2\text{Ti}_2\text{O}_7$  (EYYTO) phosphor ( $\lambda_{\text{em}} = 548$  nm,  $\lambda_{\text{exc}} = 976$  nm).

It is defined as time duration in which the population of higher energy level state is reduced by 1/e of its initial population associated with involved transitions from higher energy to the lower energy state. The measured decay curves were fitted to the equation as

$$I(t) = I_0 \exp\left(\frac{-t}{\tau}\right) \quad (3.2)$$

where  $\tau$  is the life time of emitting level. The decay data is found to fit well with mono-exponential fitting having goodness of fit  $R^2 = 0.9968$ . The calculated value of life time of <sup>4</sup>S<sub>3/2</sub> level is found to be ~446  $\mu$ s, which is slightly low to value reported by Ting et al.(2011) for Er<sup>3+</sup> doped YTO. The shorter value of life is attributed to occurrence of energy transfer from Yb<sup>3+</sup> → Er<sup>3+</sup> and the proposed energy transfer processes are quite reasonable for the EYYTO sample.

In last few years several results have been reported for different Er<sup>3+</sup> or Er<sup>3+</sup>/Yb<sup>3+</sup> co-doped systems widely studied through up-conversion processes (i.e., BaTiO<sub>3</sub>, TiO<sub>2</sub>, Y<sub>2</sub>O<sub>3</sub> etc) [Camargo, et al. (2007), Patra, et al (2003b)]. YTO shows comparable phonon frequency to the other hosts like BaTiO<sub>3</sub>, TiO<sub>2</sub> and Y<sub>2</sub>O<sub>3</sub>, and having higher thermal & mechanical stability, higher refractive index and wide band gap open its broad and multifunctional applicability. The crystallinity will appear in Er<sup>3+</sup> doped TiO<sub>2</sub> and BaTiO<sub>3</sub> samples at ~500 and 700 °C annealing temperature, respectively. Reports show the presence of anatase and rutile phases in case of Er<sup>3+</sup> doped TiO<sub>2</sub> host between 500-1000 °C annealing temperatures. Optimum up-conversion emission intensity found at around at ~800 °C for TiO<sub>2</sub> host and increases with annealing temperature in case of BaTiO<sub>3</sub>. Recently luminescence properties of Eu<sup>3+</sup> doped Y<sub>2</sub>Ti<sub>2</sub>O<sub>7</sub> have been reported via solvothermal process; particles show amorphous nature upto ~750 °C annealing temperature [Pavitra, et al.(2012)]. The present EYYTO phosphor shows tunable up-conversion emission and high crystallinity. This material can be used extensively in opto-electronic device applications. Also less effort is made to prepare colloidal solution of EYYTO phosphor sample. This solution can be easily dispersed in polymer thin films and it can be coated on solar cell device for enhancing the solar cell efficiency.

### 3.4 Conclusions

The  $\text{Er}^{3+}/\text{Yb}^{3+}$  co-doped yttrium titanate nanophosphors were prepared by using solid state reaction route and characterized their comparative structural and up-conversion properties. Some strong green and red emission transitions were observed at  $\sim 524$ ,  $548$  and  $661$  nm which originating from electronic transitions ( ${}^2\text{H}_{11/2} \rightarrow {}^4\text{I}_{15/2}$ ,  ${}^4\text{S}_{3/2} \rightarrow {}^4\text{I}_{15/2}$  and  ${}^4\text{F}_{9/2} \rightarrow {}^4\text{I}_{15/2}$ ) of  $\text{Er}^{3+}$ , respectively. The power dependence studies of these bands, infer that they arise through two photon absorption process. The PL properties of  $\text{Er}^{3+}/\text{Yb}^{3+}$  doped samples prepared via laser ablation method shows the dominance of red band over green band. It also shows strong absorption band near  $1.45 \mu\text{m}$ , which makes this useful for possible laser material in optical communication system. The CIE coordinate varies with input laser power which dictates the color tunability of the material. Photoluminescence decay of green band at  $\sim 548$  nm is studied and found to be mono-exponential in nature. The slightly smaller value of life time of this  ${}^4\text{S}_{3/2}$  is attributed to the energy transfer from  $\text{Yb}^{3+} \rightarrow \text{Er}^{3+}$  and inhomogeneity present in the  $\text{Er}^{3+}/\text{Yb}^{3+}$  doped YTO host.

★★★★★★